# Self-assembly, condensation, and order in aqueous lyotropic chromonic liquid crystals crowded with additives†

Luana Tortora,[a] Heung-Shik Park,[ab] Shin-Woong Kang,[d] Victoria Savaryn,[ab] Seung-Ho Hong,[c] Konstantine Kaznatcheev,[e] Daniele Finotello,[acf] Samuel Sprunt,[ac] Satyendra Kumar[abc] and Oleg D. Lavrentovich*[ab]

*Received 5th March 2010, Accepted 8th June 2010*
**DOI: 10.1039/c0sm00065e**

Dense multicomponent systems with macromolecules and small solutes attract a broad research interest as they mimic the molecularly crowded cellular interiors. The additives can condense and align the macromolecules, but they do not change the degree of covalent polymerization. We chose a lyotropic chromonic liquid crystal with reversibly and non-covalently assembled aggregates as a much softer system, reminiscent of "living polymers", to demonstrate that small neutral and charged additives cause condensation of aggregates with ensuing orientational and positional ordering and nontrivial morphologies of phase separation, such as tactoids and toroids of the nematic and hexagonal columnar phase coexisting with the isotropic melt. Scanning transmission X-ray microscopy (STXM) with near edge X-ray absorption fine structure (NEXAFS) analysis as well as fluorescent microscopy demonstrates segregation of the components. The observations suggest that self-assembly of chromonic aggregates in the presence of additives is controlled by both entropy effects and by specific molecular interactions and provide a new route to the regulated reversible assembly of soft materials formed by low-molecular weight components.

## Introduction

Molecular assembly in dense multicomponent systems that closely mimic the molecularly crowded cellular interiors, is a fascinating problem that has been actively studied over the last few decades. In the approach pursued by physicists, the focus is primarily on water solutions of macromolecules (polymers, proteins and nucleotides) in the presence of "small" solutes such as neutral polymers, alcohols, simple and multivalent salts. The additives condense and align the macromolecules, either through the excluded volume effects or electrostatically. The macromolecules are driven together but their degree of covalent polymerization remains intact. In the biochemical studies, the focus is primarily on complex chemical reactions that involve formations of strong covalent bonds. In this work we explore a much softer system, a lyotropic chromonic liquid crystal (LCLC), in which small molecules are reversibly assembled into aggregates by weak non-covalent forces.

Chromonic aggregation is featured by aqueous solutions of many organic molecules with aromatic cores and ionic groups at the periphery. The family is broad and includes drugs, dyes[1–4] and nucleic acids.[5,6] The individual plank-like molecules reversibly assemble into one-dimensional elongated aggregates (living polymers) by stacking face-to-face and leaving the charged groups at the aggregate–water interface. The face-to-face stacking energy $E$ is only a few units of Boltzmann thermal energy $k_BT$, much lower than the typical covalent bond energy. As the concentration increases, the aggregates multiply, elongate, and align parallel to each other, forming a nematic (N) or a columnar (C) phase with hexagonal positional order.[1,2]

In this work, we demonstrate experimentally that the order and morphology of weak non-covalent chromonic assembly can be effectively controlled by crowding the solutions with neutral and weakly charged additives. Prior experiments[7–10] focused mostly on electrostatic effects of additives. Monovalent and divalent salts such as NaCl, KCl, and $MgSO_4$ added to the LCLC, typically expand the temperature and concentration range of the N phase[7–10] by screening intra- and inter-aggregate electrostatic repulsion. Neutral additives such as poly (ethylene glycol) (PEG) are known to condense and align macromolecular DNAs[11–14] and self-assembled guanosine aggregates[6] through the excluded volume effects, in the presence of salts. A theoretical framework has been laid down by Madden and Herzfeld[15,16] who numerically simulated a mixture of aggregating chromonic and neutral non-aggregating spheres and predicted that the two species should demix into a liquid crystalline (LC) domain with a high concentration of chromonics and an isotropic (I) phase enriched in non-aggregating spheres. However, for oligomeric DNAs capable of chromonic self-assembly, PEG was reported to cause a liquid–liquid phase separation[14] rather than the liquid–LC phase separation expected on the basis of

[a]*Liquid Crystal Institute, Kent State University, Kent, Ohio, 44242, USA. E-mail: olavrent@kent.edu; Fax: + 1 33 0672 2654; Tel: +1 33 0672 4844*
[b]*Chemical Physics Interdisciplinary Program, Kent State University, Kent, Ohio, 44242, USA*
[c]*Department of Physics, Kent State University, Kent, Ohio, 44242, USA*
[d]*Department of BIN Fusion Technology, Chonbuk National University, Jeonju, South Korea 561-756*
[e]*NSLSII project, Brookhaven National Laboratory, Upton, New York, 11973, USA*
[f]*Division of Materials Research, National Science Foundation, Arlington, Virginia, 22230, USA*
† Electronic supplementary information (ESI) available: Scanning Transmission X-ray Microscopy. See DOI: 10.1039/c0sm00065e

theory.[15,16] Luk *et al.*[17] reported that the neutral PEG does not cause phase separation in isotropic solutions of LCLC materials, but other water-soluble nonionic polymers, such as polyvinyl alcohol, lead to stable emulsions of LCLC droplets in water. Anionic polysodium 4-styrenesulfonate and cationic polyethyleneimine lead to unstable emulsions and precipitation, respectively.[17] Note also that the LCLC columnar phases have been demonstrated to be non-miscible with their counterparts formed by amphiphilic molecules.[18]

Despite the fact that very little is known about the behavior of ternary systems LCLC/water/additive, there is a substantial amount of knowledge accumulated on the related issue of condensation of DNA and also on condensation in the system surfactant/additive/water, when the additive does not dissolves in the surfactant phase, see, *e.g.*, ref. 19.

The LCLC material disodium cromoglycate ((1) DSCG, Fig. 1) and three different additives, multivalent spermine free base ((2) Spm, Fig. 1), monovalent tetrabutylammonium bromide ((3) TBABr, Fig. 1) and an electrically neutral PEG ((4), Fig. 1) were chosen based on the following considerations. First, DSCG is optically transparent and its phase state and orientation of aggregates can be traced by optical techniques, such as polarized light or optical retardance microscopies. Second, PEG and Spm can be chemically modified with a fluorescent probe attachment, thus their spatial distribution in a sample can be monitored by a fluorescence microscope. Third, elemental composition of DSCG and additives is sufficiently different (DSCG contains oxygen atoms but no nitrogen, while the opposite is true for TBABr and Spm) to employ the newly developed technique of scanning X-ray transmission microscopy (STXM) and map the spatial distribution of DSCG and additives in phase separated regions without any chemical modification.

## Experimental

### Materials

DSCG, also known as cromolyn and INTAL, of chemical name disodium 5,5′-[(2-hydroxy-1,3-propanediyl)-bis(oxy)]-bis[4-oxy-4*H*-1-benzopyran-2-carboxylate] of purity 98% was purchased from Spectrum and used without further purification. Spm freebase (purity ≥ 99%) was purchased from Sigma-Aldrich. TBABr (purity ≥ 98%, Sigma-Aldrich) is a monovalent quaternary ammonium salt whose state of charge is not influenced by pH as the central nitrogen is linked to four alkyl groups. PEG of molecular weight 3350 was purchased from Sigma-Aldrich. Deionized water (resistivity of ≥18.0 MΩ cm) was used for preparation of all solutions.

A fluorescent version of PEG, fluorescein isothiocyanate PEG (FITC-PEG), of molecular weight 3400 was purchased from Nanocs. A fluorescent version of Spm was synthesized by covalently attaching fluorescein isothiocyanate (FITC, purchased from Sigma-Aldrich) to Spm and forming Spm trihydrochloride (FITC-Spm$Cl_3$).[20]

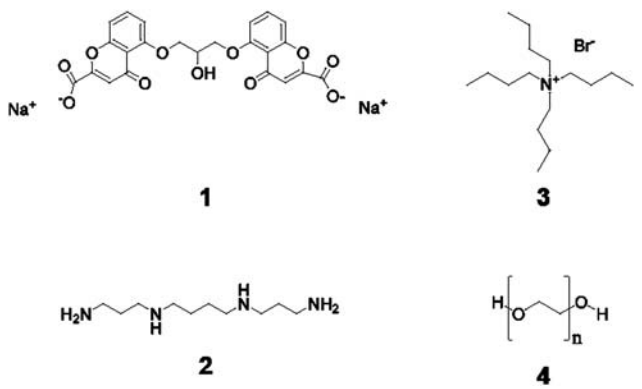


**Fig. 1** Molecular structures of (1) DSCG, (2) Spm, (3) TBABr and (4) PEG.

### Methods

**Polarized optical microscopy (POM).** We used glass cells with a fixed gap $h$ measured by interference technique prior to filling. The typical thickness of cells used to construct the phase diagrams was 12 μm and in the case of PolScope measurements, $h \approx 3$ μm. The glass plates yield tangential orientation of the director $\hat{\boldsymbol{n}}$ specifying the average orientation of LCLC aggregates. To promote a unidirectional planar alignment for measurements of refractive indices, the plates were covered with buffed layers of polyimide SE-7511 (Brewer Science). The phase diagram was determined upon cooling (rate $-0.5$ °C min$^{-1}$) in a hot stage TMS94 (Linkam).

**Abrio LC-PolScope and refractive index measurements.** The LC-PolScope[21] was used to measure optical retardance $R = h|\Delta n|$ at wavelength 546 nm and to map orientation of the slow axis, which is *normal* to $\hat{\boldsymbol{n}}$ for DSCG solutions. Here $\Delta n = n_e - n_o < 0$ is (negative) birefringence of the solution, $n_o$ and $n_e$ are the ordinary and extraordinary indices of refraction, respectively. The negative sign of $\Delta n$ was directly established in separate experiments performed on wedge-like cells of DSCG solutions with $\hat{\boldsymbol{n}}$ perpendicular to the thickness gradient. The birefringent prism allows one to measure $n_o$ and $n_e$ by observing deflection of linearly polarized (parallel and perpendicular to $\hat{\boldsymbol{n}}$) laser beams propagating through the prism, and to establish that $n_e - n_o < 0$. The latter implies that the optical slow axis mapped by LC-PolScope is perpendicular to $\hat{\boldsymbol{n}}$.

**Density measurements.** A density meter Mettler Toledo DE45 was used to determine the density $\rho$ of DSCG solutions in homogeneous N and C phases.

**Synchrotron X-ray identification of the LC phases and characterization of DSCG.** The analysis was performed at the Advanced Photon Source of Argonne National Laboratory, as described in ref. 9. Additional X-ray studies were conducted on the beam line X6B, at the National Synchrotron Light Source, Brookhaven National Laboratory. LCLC samples were sealed in 1 mm diameter, 0.01 mm wall fused quartz capillaries. These were loaded into an aluminium cassette with a 1.5 mm clearance hole to accommodate the 0.2 × 0.3 mm incident X-ray beam and to allow ±13.5° angular access. Stacked NdFeB magnets were used to produce a ~15 kG field across the capillary,

sufficient to align the LCLC. The cassette was placed into a temperature regulated hot-stage, which was housed in an evacuated chamber. Scattering was recorded on a 2084 × 2084 element Princeton Instruments area detector positioned 1.2 m from the sample. The effective $q$-resolution of the experiment was 0.00331 $Å^{-1}$. For the C phase, the lattice parameter $D$ is calculated as $D = 2d_1/\sqrt{3}$, where $d_1$ is the first X-ray diffraction line, so that $D$ represents the inter-aggregate axis-to-axis distance; note that the coefficient $2/\sqrt{3}$ is often omitted when the spacing is discussed for both C and N phases, as in ref. 9.

**Soft X-ray spectromicroscopy.** Measurements were performed at the Canadian Light Source scanning transmission X-ray microscope (STXM) with the near edge X-ray absorption fine structure (NEXAFS) analysis, as described in ref. 22 and ESI†. NEXAFS is an electron spectroscopic technique based on the absorption of an X-ray photon by a core level of an atom; it is element-specific and sensitive to orientation of bonds. We used linearly polarized soft X-ray light focused into a ~50 nm focal spot. The intensity of NEXAFS resonances depends on the angle between the polarization of X-ray and the transition moment vector. For $K$-edge absorption, where the core electron density distribution is atomic-like and the dipole transition moment polarization selection rules are dictated by the symmetry of an unoccupied orbital, the dichroic NEXAFS signal provides a direct measurement of the given bond orientation. By measuring the sequence of images with varying polarization of X-ray, we mapped the in-plane linear dichroism and thus the average orientation of the molecular bonds and an order parameter associated with them, with the spatial resolution below 100 nm.[22]

The STXM measurements impose several restrictions on sample preparation. One of them is caused by strong absorption of water at photon energies above 535 eV, with optical density approaching 4.5 per micron at 538 eV. It was still possible to deduce the orientational order of DSCG, by monitoring how the lower energy 531.4 eV NEXAFS peak associated with C═O bonds of DSCG molecules depends on polarization of X-rays impinging normally onto the sample. We used two types of samples, "wet" and "dry", in STXM-NEXAFS studies. The wet samples were prepared by placing a droplet of LCLC (with the additives) onto a face of $Si_3N_4$ window and then quickly covering it with another $Si_3N_4$ plate and sealing the cell. In wet samples, water was present during the STXM examination, although at somewhat reduced concentration. To improve the $Si_3N_4$ membrane wettability, Si chips were pretreated in a plasma (air) etcher. The second type, called "dry film" samples, were prepared by spreading a droplet of LCLC solution on a face of $Si_3N_4$ window with a razor blade. The deposition forces the LCLC director to align tangentially to the substrates, along the shear direction.[22] No cover plate was used in these "dry" samples, *i.e.*, water was allowed to evaporate. The sample was placed in the STXM chamber that was pumped to $10^{-2}$ Torr to evacuate air and then filled with helium to 0.2 atmosphere. We explored the dry samples of both additive-free (the data are presented in the ESI†) and crowded solutions of DSCG. In the latter case, phase separation occurred before drying and the resulting textures showed features remarkably similar to those of phase separated wet samples.

**Fluorescent confocal microscopy.** To get an additional insight into the spatial distribution of components in the phase separated mixtures of DSCG, we used very small quantities of fluorescent crowding additives, which were added to their non-fluorescent counterparts. For observations, we used an Olympus Fluoview BX-50 confocal microscope. No drying was involved in this case.

## Results

We study the effects of additives on water solutions of DSCG with concentrations $c = 0.29$ mol $kg^{-1}$ (or 13 wt% or in molar units $[c] = 0.27$ mol $L^{-1}$) and $c = 0.34$ mol $kg^{-1}$, as these exhibit a homogeneous N phase close to the room temperatures.[23,24] The data for the two were qualitatively similar. Fig. 2 shows how birefringence $\Delta n = n_e - n_o < 0$ (measured at 546 nm) and density $\rho$ of the additive-free DSCG solutions depend on $c$ and $T$; these data will be used in getting an insight into the structure of the condensed regions.

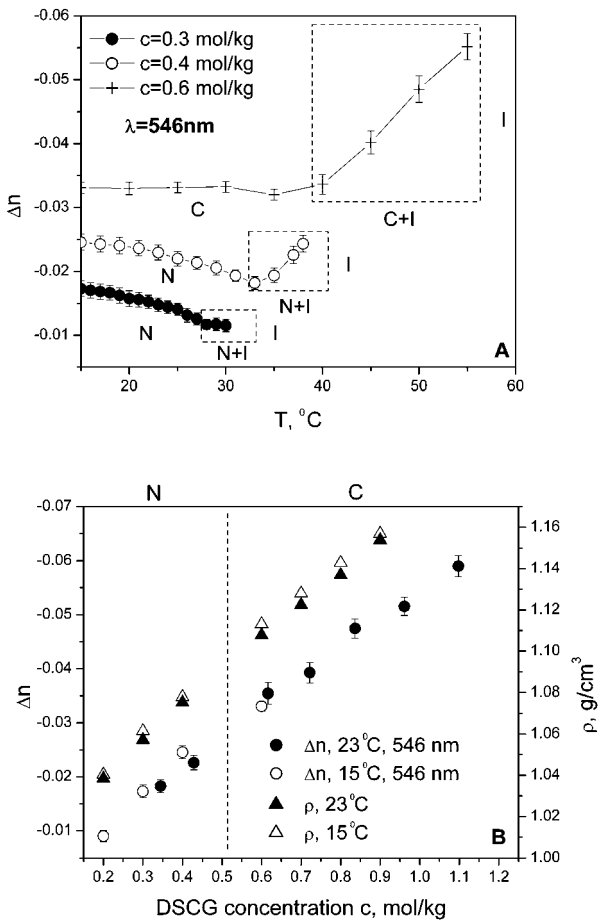


**Fig. 2** (A) Temperature dependence of birefringence $\Delta n$ for DSCG solutions with $c = 0.3$ mol $kg^{-1}$ (bottom curve), 0.4 mol $kg^{-1}$, 0.6 mol $kg^{-1}$ (top curve), all measured with 546 nm light; letters N, C and I label the nematic, columnar and isotropic phases, respectively; (B) Concentration dependencies of $\Delta n$ and density $\rho$ for DSCG solutions at 15 °C and 23 °C.

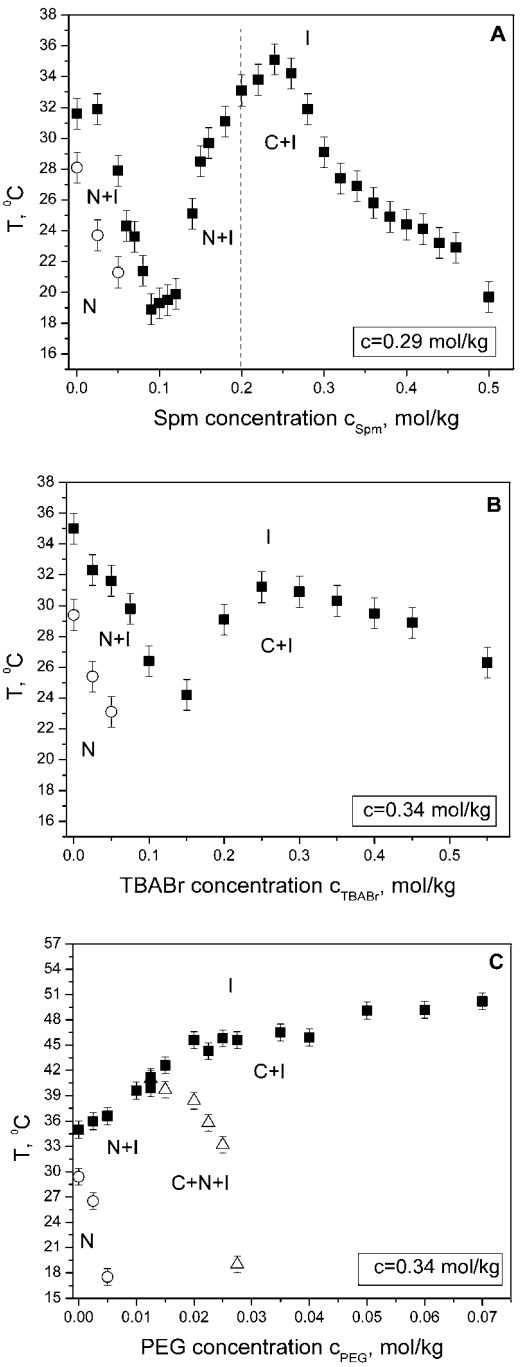


**Fig. 3** The phase diagram of DSCG solutions with added Spm (A), TBABr (B) and PEG (C). In (A), $c = 0.29$ mol kg$^{-1}$; in (B) and (C), $c = 0.34$ mol kg$^{-1}$. The filled squares mark the transformation of the homogeneous I phase into the biphasic regions with birefringent N and C inclusions. The circles mark the formation of a homogeneous N phase from the biphasic N + I state. The triangles mark the appearance of the N inclusions in the samples with coexisting C + I phases. The vertical dashed line in (A) represents a tentative boundary between the N + I and C + I coexistence domains.

### Additive-induced condensation, orientational and positional order

At low concentrations, Spm ($c_{Spm} < 0.08$ mol kg$^{-1}$) suppresses the orientational order and reduces the temperatures of phase transitions, Fig. 3A. At intermediate concentrations, Spm condenses DSCG into the more birefringent N phase or even into the hexagonally ordered C phase, both coexisting with the I phase. At $c_{Spm} > 0.25$ mol kg$^{-1}$, the LC order is destroyed, Fig. 3A. All the phase transition temperatures were recorded on cooling. The transitions are reversible, in the sense that they do not lead to irreversible precipitation.

TBABr produces effects qualitatively similar to that of Spm (Fig. 3B) while the effect of PEG is different. PEG causes condensation of the LCLC domains in the entire range of studied concentrations, Fig. 3C. Increasing $c_{PEG}$ leads to a higher melting temperature. For a fixed temperature, say, $T = 38$ °C, the pure DSCG solution is isotropic, but in the presence of PEG, it condenses into the N and even the C phase. The phase identification in Fig. 3 is confirmed by the X-ray diffraction data.

### Shape morphologies of condensation

The additives-induced phase separation of the type N + I (low concentration of additives $c_{Add}$) and C + I (high $c_{Add}$) shows different shape morphologies and director patterns, Fig. 4.

The N + I regions feature tactoids,[24,25] with $\hat{\boldsymbol{n}}(\boldsymbol{r})$ being tangential to the N–I interface and showing splay (near the poles) and bend (near the equator), Fig. 4A. The structure is established by the LC-PolScope mapping of the slow axis[21] that is perpendicular to $\hat{\boldsymbol{n}}(\boldsymbol{r})$. Near $c_{Spm} = 0.175$ mol kg$^{-1}$, the tactoids coexist with toroid-like structures, Fig. 4B, with a complex director pattern that deserves further studies. The condensed C inclusions show a variety of shapes, such as flexible bundles, Fig. 5B, and toroids, Fig. 4C, in which $\hat{\boldsymbol{n}}(\boldsymbol{r})$ prefers bend deformation and tangential surface alignment at the C–I interface. The toroids with a circular $\hat{\boldsymbol{n}}(\boldsymbol{r})$ represent an ideal example; they are frequently formed by merging of the two ends of elongated bundles. Some of the C phase shapes are close to those described theoretically by Starostin for hexagonally ordered DNA.[26] The typical radius of the C-toroids, $R \approx 10$ μm, is much larger than the radius 50–100 nm of condensed DNA toroids.[12] The aspect ratio, $R/r$ of toroids and tactoids is significantly larger than 1, Fig. 4A, B and C. In tactoids, $R$ is the long and $r$ is the short semiaxis; in toroids, $R$ is the radius of toroid and $r$ is the radius of toroidal tube, Fig. 4D.

### Birefringence and packing density in condensed regions

In Fig. 5A, we plot birefringence $\Delta n$ of the condensed regions measured using the LC-PolScope as a function of $c_{Spm}$. The birefringence was measured locally for condensed regions that are wider than the cell gap $h$, Fig. 5B. For $c_{Spm} < 0.08$ mol kg$^{-1}$, $|\Delta n|$ decreases with $c_{Spm}$, but the sample remains homogeneous, suggesting that Spm disorders the N phase from within it. For $c_{Spm} > 0.09$ mol kg$^{-1}$, $|\Delta n|$ measured inside the condensed regions increases with $c_{Spm}$, reflecting the phase separation of the type N + I and, above $c_{Spm} = 0.19$ mol kg$^{-1}$, of the type C + I. The dependency $\Delta n(c_{Spm})$ suggests that the distance $D$ between

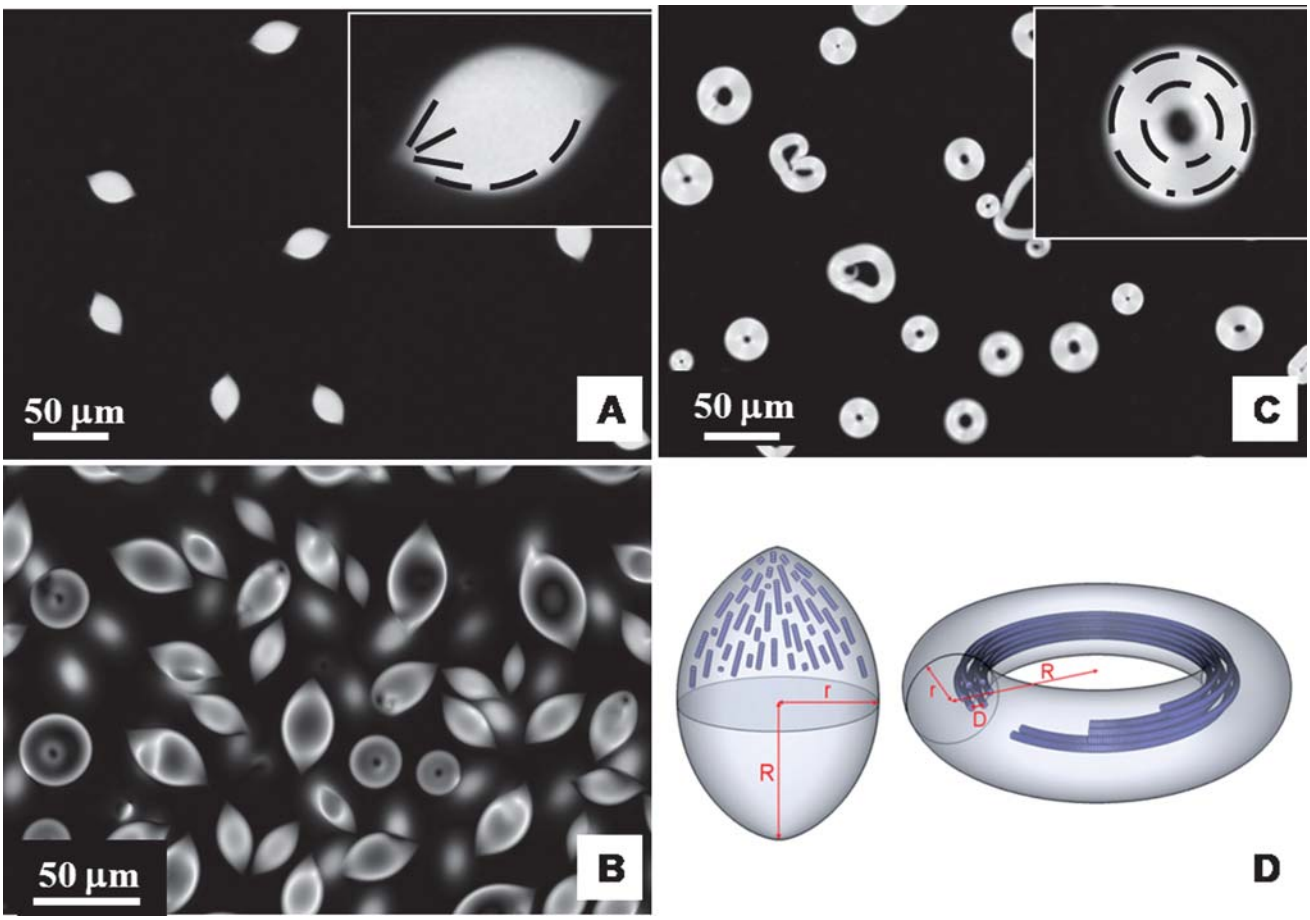


**Fig. 4** DSCG solution with $c = 0.34$ mol kg$^{-1}$ phase separates in the presence of Spm into different morphologies: (A) $c_{Spm} = 0.150$ mol kg$^{-1}$, N tactoids with splay of director near the poles and bend near the equator; (B) $c_{Spm} = 0.175$ mol kg$^{-1}$, coexisting tactoids and toroid-like structures; (C) $c_{Spm} = 0.2$ mol kg$^{-1}$, C toroids with bend distortions and bundles; (D) scheme of director distortions inside an N tactoid and a C toroid. The LC-PolScope images are taken at 23 °C. The insets in parts (A) and (C) show enlarged N tactoid and C toroid with the director distortions reconstructed from LC-PolScope observations.

the DSCG aggregates in the condensed regions decreases with $c_{Add}$.

A good insight into the issue of additive-induced denser packing of aggregates is provided by considering the C condensates only, since in this case the value of $D$ is well defined and can be determined either indirectly, from the $\Delta n$ data, following the model,[23] or directly by X-ray diffraction measurements, Fig. 6. For $c = 0.29$ mol kg$^{-1}$, we calculate $D$ using the model,[23] in which the DSCG aggregates are formed by face-to-face stacking of DSCG molecules. According to, ref. 23 the columnar cylindrical aggregates of diameter $d = 1.6$ nm are packed in the hexagonal array, so that $D = d\sqrt{\pi/(2\sqrt{3}\eta)}$, where $\eta = \left[1 - \frac{V_w}{V_{DSCG}}\left(\frac{1-W}{W}\right)\right]^{-1}$, $V_w$ and $V_{DSCG}$ are the partial specific volumes of water and DSCG, respectively, $W$ is the weight fraction of DSCG, determined by comparing $\Delta n$ in the condensed regions, Fig. 5A, with the calibration curve $\Delta n(c)$ in Fig. 2. The partial specific volumes are determined by plotting $1/\rho$ *vs.* $W$.

The dependencies $D(c_{Add})$ in Fig. 6 show a dramatic reduction in the inter-columnar spacing of DSCG as the concentration of additives increases. This ability to cause a denser packing of aggregates is shown by all studied additives, the neutral PEG, partially charged Spm and monovalent TBABr. As we discuss below, the most plausible mechanism for the case of PEG is the depletion effect: the PEG molecules are expelled from the condensed LCLC domains and accumulate in the I phase, thus creating an osmotic pressure that pushes the LCLC molecules and aggregates closer together. This mechanism implies that PEG and DSCG molecules are spatially separated, with DSCG predominantly filling the birefringent condensed N and C regions and PEG concentrating in the I phase. As shown below, for Spm and TBABr, we also find the experimental evidence of spatial separation of the components. However, the positively charged additives can contribute to the phase separation not only through the excluded volume effect, but also through electrostatically mediated association with the negatively charged DSCG molecules. In the remaining three sections we characterize the structure of phase separated domains and spatial distribution of the components using X-ray and fluorescent microscopies.

### Orientation of DSCG molecules in the condensed regions

The arrangement of DSCG molecules in the LC phases is a subject of ongoing discussion since the early studies, as

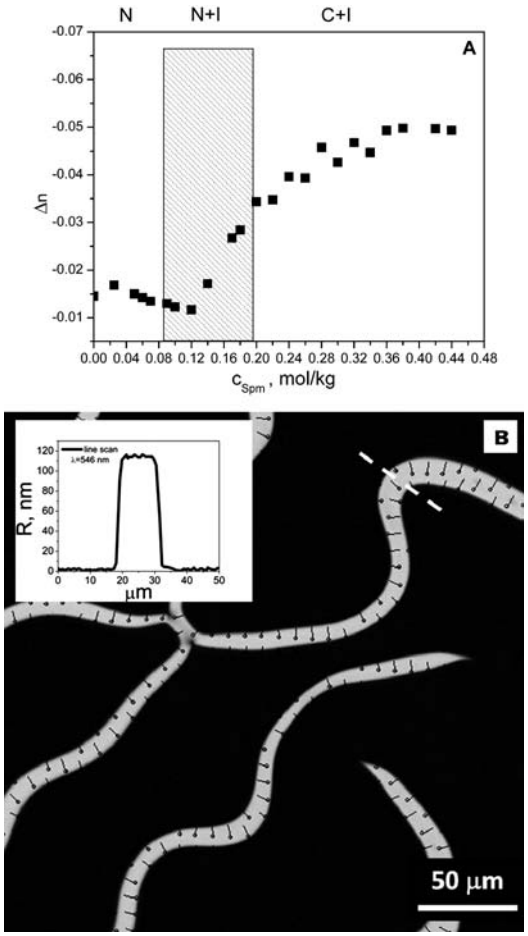


**Fig. 5** (A) Birefringence $\Delta n$ of LC regions of DSCG + Spm mixtures as a function of Spm concentration $c_{Spm}$; $c = 0.29$ mol kg$^{-1}$, 15 °C. At low $c_{Spm}$, the N phase is homogeneous, at moderate $c_{Spm}$, it separates into the coexisting N and I domains (hatched region) and at high $c_{Spm}$, it separates into the C and I domains; (B) LC-PolScope texture of birefringent condensed bundles formed in $c = 0.29$ mol kg$^{-1}$ DSCG solution after addition of $c_{Spm} = 0.24$ mol kg$^{-1}$ of Spm. The inset shows the optical retardation $R = (113 \pm 5)$ nm across the bundle (along the dashed line in the texture); $R$ is restricted by the finite thickness of the sample. The slow axis (bars) is perpendicular to the axis of bundles and to $\hat{\boldsymbol{n}}(\boldsymbol{r})$.

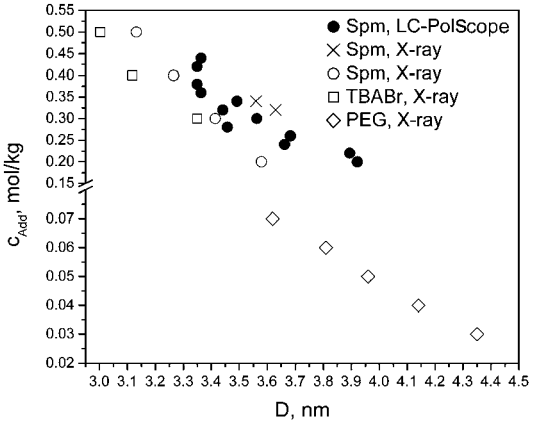


**Fig. 6** Relationship between $c_{Add}$ and the hexagonal period $D$ in the condensed C phase, for $c = 0.34$ mol kg$^{-1}$ of DSCG doped with Spm (○) and TBABr (□) as measured by X-ray diffraction; the same for DSCG $c = 0.34$ mol kg$^{-1}$ doped with PEG (◇), and for DSCG $c = 0.29$ mol kg$^{-1}$ doped with Spm, as measured by X-ray (X) and as calculated from the data on $\Delta n$ (●).

reviewed by Vasilevskaya *et al.*[27] In the highly diluted I phase, conformation of the DSCG molecules is essentially planar, with two aromatic ring groups approximately parallel to each other[28] despite the fact that these two ring systems are bridged by single bonds and thus can in principle rotate with respect to each other. In the classic picture of the LC order at higher DSCG concentration, the molecules are assembled into the rod-like columnar aggregates on top of each other, with their planes perpendicular to the axes of aggregates and to $\hat{\boldsymbol{n}}$;[23,27,29] the models consider either four[27] or two[3] molecules per cross-section of the aggregate.

Recently,[30] a new thread-like model has been proposed. In the thread model, the DSCG planes are connected side by side through "salt bridges" into "threads" rather than stack on top of each other as in the model of columnar aggregates. The threads then align parallel to each other to form an orientationally ordered N phase. To clarify the type of DSCG assembly in our case, we compared the data on birefringence and X-ray microscopy.

The negative sign of birefringence, $\Delta n = n_e - n_o < 0$ measured in the N and C phases, is consistent with the idea that the aromatic ring groups of DSCG molecules are on average perpendicular to the axis of aggregates and to $\hat{\boldsymbol{n}}$. If the ring planes were parallel to the thread-like structures and to $\hat{\boldsymbol{n}}$, then $\Delta n$ should be positive, because of the individual molecular contributions and because of the "form birefringence", see, *e.g.*, ref. 31. Another manifestation of the mutually perpendicular arrangement of the molecular planes and $\hat{\boldsymbol{n}}$ is that in the condensed C phase, the slow axis is always perpendicular to the interface with the I phase, Fig. 4C and 5B, while $\hat{\boldsymbol{n}}$ is parallel to this interface. The tangential surface alignment of $\hat{\boldsymbol{n}}$ in the flexible bundles and toroids of C phase reduces elastic distortions of the splay and twist type and maintains the flexibility through the bend of $\hat{\boldsymbol{n}}$. If the DSCG ring planes and $\hat{\boldsymbol{n}}$ were parallel, then one would observe the slow axis parallel to the N–I and C–I interfaces, which is not the case in our experiments, Fig. 4C and 5B.

A direct verification of molecular orientation with respect to $\hat{\boldsymbol{n}}$ is established by STXM with polarization-sensitive NEXAFS. We measure the polarization dependence of the O 1s → π* peak at 531.4 eV that is attributed to the excitations of groups C═O in the DSCG molecules. According to the X-ray structural studies of DSCG by Stephenson and Diseroad,[32] the carboxyl group is coplanar with the adjacent aromatic ring, so the measurement of the polarization dependence of the 1s → π* transition would adequately define orientation of the aromatic rings. The photon absorption is suppressed when the π* orbitals are perpendicular to the polarization of X-ray. The intensity of 531.4 eV line should be minimum when the polarization of X-ray is parallel to the ring planes of DSCG and maximum when it is perpendicular to them. As a reference, we use maps of dried DSCG solutions with no additives, shear-deposited onto a substrate (see ESI†). The textures are similar to the one studied in details earlier for other LCLCs[22] and demonstrate that drying essentially freezes and memorizes the orientational order rather than crystallizes the material into a completely new pattern, see also ref. 32–34. For

 

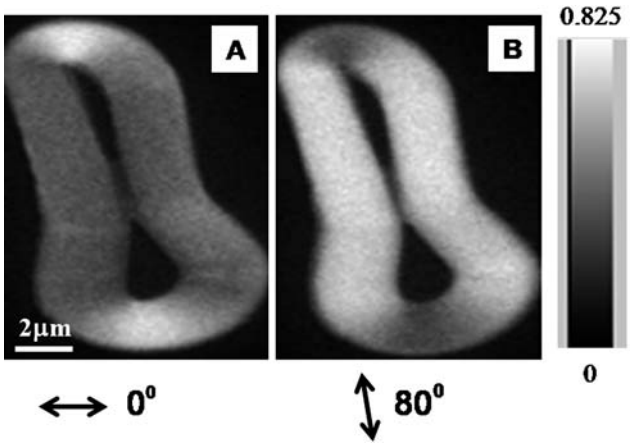


**Fig. 7** STXM NEXAFS orientational texture obtained with a linearly polarized X-ray. Wet sample, DSCG + TBABr ($c$ = 0.34 mol kg$^{-1}$, $c_{TBABr}$ = 0.3 mol kg$^{-1}$), with a condensed LC region in the shape of number "8". The textures represent polarized optical density OD = ln($I_0$/$I$) images at the fixed energy of 531.4 eV, with the direction of linear polarization (shown by the double arrow) set at 0° (A) and 80° (B) with respect to the horizontal line; OD is maximum whenever the X-ray is polarized perpendicularly to the molecular plane, *i.e.*, parallel to the director $\hat{\boldsymbol{n}}$.

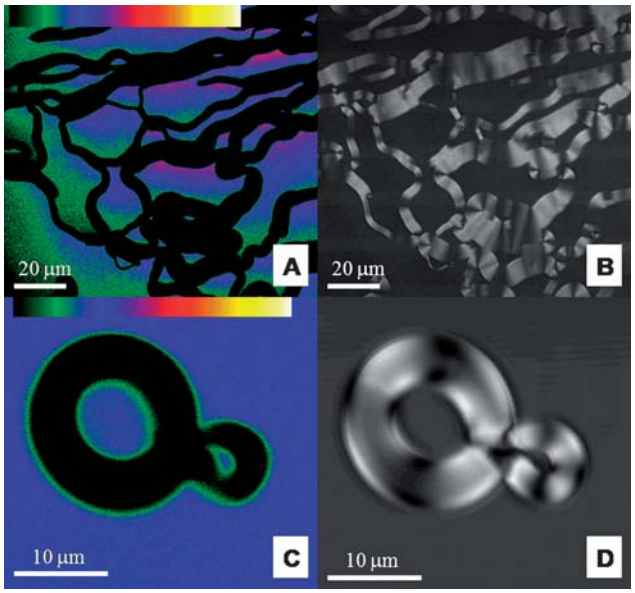


**Fig. 8** (Color) Demixing and condensation in the aqueous solutions of DSCG caused by fluorescent additives, as viewed by fluorescent (left column) and regular polarizing (right column) microscopes: (A and B) $c$ = 0.31 mol kg$^{-1}$, with an addition of PEG, $c_{PEG}$ = 0.016 mol kg$^{-1}$, and 8 × 10$^{-5}$ mol kg$^{-1}$ of FITC-PEG; (C and D) $c$ = 0.34 mol kg$^{-1}$ with an addition of $c_{Spm}$ = 0.25 mol kg$^{-1}$ Spm and 2.8 × 10$^{-4}$ mol kg$^{-1}$ of FITC-SpmCl$_3$; temperature 23 °C. In the left column, black regions represent the lowest concentration of fluorescent dye, and colors from green to yellow as indicated on the top bar correspond to an increased concentration of fluorescent additive. In the right column, the bright regions correspond to the birefringent C phase, while the I regions are uniformly dark. Note the complementary nature of the images: the black regions in fluorescence images (A and C) correspond to birefringent domains of polarizing microscope pictures (B and D) and dark areas of POM correspond to dye-rich colored regions in fluorescent textures.

shear-aligned DSCG with no additives, the peak at 531.4 eV is maximum when the beam is polarized along the shear direction, indicating that the aromatic ring planes of DSCG molecules are perpendicular to $\hat{\boldsymbol{n}}$, Fig. S2†.

The perpendicular arrangement of DSCG planes and $\hat{\boldsymbol{n}}$ is evident not only in the additive-free samples, but also in the structure of LC regions condensed by additives, as illustrated in Fig. 7 for the wet sample with a condensed birefringent C region in the shape resembling number "8". The optical density OD = ln($I_0$/$I$) is maximum (corresponding to brighter regions in Fig. 7) whenever the X-ray polarization is perpendicular to the molecular plane, thus parallel to the director $\hat{\boldsymbol{n}}$. We conclude that in the liquid crystalline phases of DSCG, both pure and condensed by additives, the DSCG molecules are predominantly perpendicular to the interface with the I phase and perpendicular to the director. As shown below, Fig. 9B and E, the DSCG molecular planes remain perpendicular to the director also in the dry films.

### Spatial partitioning of additives and chromonics

Segregation of additives and DSCG is evident in fluorescent microscopy observations of mixtures doped with fluorescent versions of the additives. Fig. 8 shows fluorescence (left) and polarized optical microscope textures (right) of the $c$ = 0.31 mol kg$^{-1}$ solution of DSCG, doped with PEG, $c_{PEG}$ = 0.016 mol kg$^{-1}$, and a small quantity, 8 × 10$^{-5}$ mol kg$^{-1}$, of FITC-PEG (Fig. 8A and B). The dark regions of the fluorescence texture (no measurable concentration of FITC-PEG) perfectly match the birefringent regions of the POM texture rich in DSCG. A similar result was obtained for the DSCG solutions with $c$ = 0.34 mol kg$^{-1}$, doped with $c_{Spm}$ = 0.25 mol kg$^{-1}$ of Spm and, in addition, with 2.8 × 10$^{-4}$ mol kg$^{-1}$ of FITC-SpmCl$_3$ (Fig. 8C and D). The fluorescence data in Fig. 8 thus demonstrate that the liquid crystalline domains contain smaller amount of the fluorescent additives and that these additives concentrate in the I phase of the phase separated samples.

STXM with NEXAFS provides a direct information on spatial distribution of DSCG and additives. This spectral analysis technique tracks separately the oxygen-containing DSCG and nitrogen-containing additives Spm and TBABr. The advantage is that no artificial labels are involved, and that one can quantify the relative concentrations of DSCG and additives, at the cost of dealing with the dried samples.

As explained in the "Methods" section, absorption of water prevented us from studying the properly diluted samples. In STXM, we used the "wet" (Fig. 7) and "dry" (Fig. 9) samples with a reduced amount of water. The dry samples were dehydrated after the additives-induced phase separation has been completed. Despite the difference in water content, all samples show similar features regarding the additive-induced phase separation and orientational order. In particular, in all samples the DSCG molecular planes are perpendicular to the local direction of the condensed bundles with high (and negative) birefringence. This similarity in the behavior of hydrated and dry samples is consistent with the previous studies[22,32–34] that demonstrate relatively small changes in the type of molecular arrangement upon dehydration of the LCLCs. The studies have shown that the "dry" state of DSCG still contains a substantial

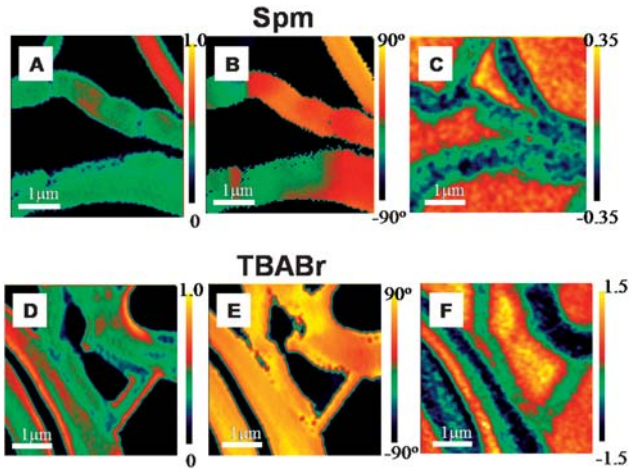


**Fig. 9** (Color) STXM NEXAFS orientational textures and maps of component distribution for dried film cast out of DSCG + Spm ($c$ = 0.34 mol kg$^{-1}$, $c_{Spm}$ = 0.3 mol kg$^{-1}$) aqueous solution (top row, A, B and C) and DSCG + TBABr ($c$ = 0.34 mol kg$^{-1}$, $c_{TBABr}$ = 0.3 mol kg$^{-1}$) solution (bottom row, D, E and F). (A and D) map relative magnitudes of the normalized scalar order parameter, as derived from the X-ray polarization measurements. Unity value corresponds to the perfectly ordered film with $\hat{\boldsymbol{n}}(\boldsymbol{r})$ = const in the plane of the film, zero to a film with random in-plane molecular orientation; (B and E) show the pseudo-color maps of the in-plane $\hat{\boldsymbol{n}}$. The colors label the angle between $\hat{\boldsymbol{n}}$ and the horizontal axis; positive angle counts as CW direction; zero corresponds to the horizontal $\hat{\boldsymbol{n}}$; the director is everywhere parallel to the boundary separating the condensed regions from the I phase; (C and F) maps of relative concentration log $c_{Add}/c$.

amount of water (up to nine molecules per DSCG molecule, depending on the humidity).[32,34] We thus expect that the dry films still preserve the basic features of phase separation in the properly diluted solutions, as additive-induced condensation and phase separation are completed before the samples are prepared for the STXM studies.

The STXM textures of phase separated samples show the DSCG-rich condensed liquid crystalline regions and the isotropic DSCG-depleted regions. Fig. 9A and D show the relative magnitude of orientational order, Fig. 9B and E show the orientation of $\hat{\boldsymbol{n}}(\boldsymbol{r})$ in the condensed regions and Fig. 9C and F show the normalized concentration ratio log $c_{Add}/c$ relative to a DSCG + Spm (top row) and DSCG + TBABr (bottom row) phase separated samples. The areas outside the condensed bundles show no orientational order. In the X-ray maps, Fig. 9A, B, D and E, we chose to mask these outside I regions in black and show only the condensed DSCG bundles. Inside the condensed regions of DSCG, the degree of orientational order is close to that one observed in DSCG dry films with no additives.[22] This is expected if the drying film and bundles have a similar composition, *i.e.* mostly filled with DSCG. Previous studies of a similar LCLCs demonstrate that the scalar order parameter changes only slightly during film transformation from the C phase into the dry state.[22]

The maps of additive distribution, Fig. 9C and F, show that Spm and TBABr are mostly expelled from the bundles into the I regions, with some amounts remaining within and probably on top of the condensed bundles. The ratio of concentrations of additives outside and inside the bundles can be estimated for Spm as $c^{OUT}_{Spm}/c^{IN}_{Spm} \approx 10^{0.7} \approx 5$, Fig. 9C, while for TBABr this ratio is noticeably larger, $c^{OUT}_{TBABr}/c^{IN}_{TBABr} \approx 10^{3}$, Fig. 9F.

## Discussion

The phase behavior of additive-free LCLCs is well described by the excluded volume model.[35] The free energy is comprised of three terms: a term favoring attraction and stacking of monomers into aggregates; a term describing inter-aggregate repulsion, with a screened electrostatic long-distance shoulder and a hard–core short-distance component, and, finally, an entropy contribution favoring disordering and dissociation of aggregates.[35] This model was extended by Madden and Herzfeld[15,16] to describe LCLCs in the presence of non-aggregating co-solutes. The additives as well as the chromonic monomers are considered to be electrically neutral spheres, with the diameter ratio $d_{Add}/d$ = 1, ½ or 2.[15,16] In our system, $d$ = 1.6 nm corresponds to the diameter of columnar LCLC aggregates.[20] The additives contribute to the free energy only through the entropy of mixing. Although neither the additives nor the DSCG molecules can be approximated as simple spheres, the model[15,16] can be compared with the following two experimental features.

(1) According to ref. 15 and 16, at small $c_{Add}$ and $d_{Add}/d$ = 1/2, the N phase accommodates some additives without phase separation. In the experiment, we do observe a similar effect manifested by a decrease of birefringence when one increases $c_{Spm}$, Fig. 5A. From the purely geometrical point of view, Spm and TBABr molecules are sufficiently small (Spm is ~1.6 nm in length when fully extended and 0.5 nm in cross-section, while the diameter TBABr is about 1 nm) to fit in the gaps $D - d \leq 3$ nm between the DSCG aggregates. The experimental reality, however, is much richer because of the electrostatic effects. The TBABr molecules are fully dissociated and charged at practically any pH. The Spm molecules might appear in differently charged forms, depending on the pH of the solution. We measured pH = 11.1 for $c$ = 0.29 mol kg$^{-1}$ with a small amount of added Spm, $c_{Spm}$ = 0.025 mol kg$^{-1}$. Using the acid constants reported in ref. 36, we calculate that at pH = 11.1, 59% of Spm molecules are neutral; 37% are in the single-charged state, 4% are in the state $SpmH_2^{+2}$ and less that 0.03% are in higher-charged states. These rough estimates can be altered towards a higher fraction of neutral Spm by a higher value of pH (when more Spm is added) or towards a higher fraction of charged species by association of Spm with DSCG. The electrostatic interactions of negatively charged LCLC aggregates with positively charged TBABr and Spm ions might cause some additional accumulation of the charged additives in the condensed regions. In Fig. 9C and F, the effect of partitioning of TBABr between the I and LC phases appears to be stronger than that of Spm. One should remember, however, that the numerical estimates of the relative concentration of additives inside and outside the condensed regions are only tentative, as the samples could be analyzed only in the dry state. The charged and extended forms of Spm might be more compatible with the condensed regions as compared to the TBABr molecules with organic coats.

For the neutral PEG, the excluded volume effects should be the main mechanism of phase separation. For the studied PEG, the gyration diameter $2R_g \approx 4.4$ nm is large. When $2R_g > D - d$, the PEG molecules cannot penetrate the spacing between

 

the DSCG aggregates and are expelled from the condensed regions, yielding an osmotic pressure on the LCLC domains that causes more dense packing and ultimately leads to the orientationally and positionally ordered phases such as N and C. The latter is in agreement with the numerical simulations[15,16] performed for "large" additives $d_{Add}/d = 2$ and also with the very recent simulations of the mixture of rigid rods and spheres that act as the osmotic compression agents.[37] In the latter work, a sufficiently high concentration of spheres caused transformation of isotropic droplets of rods into the tactoidal drops of the N phase. An important difference of our experiments is that the "rods" are not rigid but rather self-assembled columns; the additives affect not only the alignment of already existing rods–columns but also the very formation of aggregates from individual DSCG molecules and from shorter aggregates.

A comparison of parts A, B and C in Fig. 3 shows that at low $c_{Add}$, Spm and TBABr suppress the temperature of the N + I-to-I transition, while PEG increases it. We associate this with (a) the ability of positively charged Spm and TBABr ions to partially penetrate the LCLC regions and (b) a possibility of formation of ionic pairs in which the positively charged ammonium group of Spm or TBABr is linked to the negatively charged peripheral carboxylate group in the DSCG molecule, thus preventing this molecule from participation in aggregate assembly. These effects have no analogs in the model of Madden and Herzfeld.[15,16]

(2) The experiments, Fig. 3, show that at moderate $c_{Add}$, the additives condense the chromonic aggregates and cause phase separation of the type N + I or C + I. The N and C phases can emerge even from the initially isotropic state if $c_{Add}$ is high enough. For example, in Fig. 3C, the DSCG solution is isotropic at 39 °C; however, a raising $c_{PEG}$ produces first the N domains and then the C domains. The condensation effects at moderate $c_{Add}$ are clearly reflected in higher birefringence, Fig. 5A, and shorter inter-aggregate spacing, Fig. 6. The non-aggregating additives are mostly expelled from the condensed N and C regions, as confirmed directly by STXM, although some portion might remain within these regions thanks to the electrostatic forces as mentioned above. In the model,[15,16] the reason for partitioning of the additives and LCLC is of pure geometrical (excluded volume) nature, while in our experiments, the situation is complicated by specific molecular interactions in the case of charged Spm and TBABr additives. The experiments also show other features not considered by the model.

(3) At high concentrations, above approximately 0.3 mol kg$^{-1}$, Spm and TBABr destroy both orientational and positional order, Fig. 3A and B. Our X-ray diffraction data show that at elevated levels of $c_{Spm}$ and $c_{TBABr}$, the correlation length $\xi_L$ associated with the chromonic stacking, becomes small, suggesting a destruction of DSCG aggregates. For example, for $c =$ 0.34 mol kg$^{-1}$ DSCG solutions doped with TBABr $c_{TBABr} = 0.5$ mol kg$^{-1}$, one finds $\xi_L = (2.6 \pm 0.2)$ nm, which is two times smaller than $\xi_L = (5.24 \pm 0.2)$ nm in the absence of TBABr.

We associate the suppression of the order at high $c_{Spm}$ and $c_{TBABr}$ with (a) the geometrical ability of these small molecules to penetrate the condensed regions and to bind to the DSCG aggregates thus reducing the overall order, and with (b) an electrostatic binding of charged Spm and TBABr with the molecules of DSCG, thus preventing them from aggregation. For example, the charged Spm and TBABr molecules can cap the ends of the short aggregates preventing them from elongation and incorporation in the condensed phase. PEG, on the other hand, being large and neutral, cannot penetrate the condensed regions and cannot form ionic pairs with DSCG in the I phase, so that the PEG-condensed C phase remains more stable at high concentration of PEG as compared to the C-phase in the presence of high concentrations of Spm and TBABr, Fig. 3.

(4) The inter-aggregate separation $D$ in the condensed phases strongly decreases with $c_{Add}$, Fig. 6. Since the gap between the aggregates is significant, $D - d = (1.8–3)$ nm, Fig. 6, the long-range repulsive forces between the DSCG aggregates should be attributed to screened electrostatic interactions and fluctuative (undulation) repulsion forces; the hydration and van der Waals forces are much weaker in this range, as shown for similar systems such as DNA, see, *e.g.*, ref. 38

We model the DSCG aggregates as charged cylinders with a radius $a = d/2$ and "bare" dimensionless charge density $\tau$. In DSCG, there are two negative charges per stacking distance $L_0 =$ 0.34 nm and $\tau = 2l_B/L_0 \approx 4.2$, where $l_B = e^2/4\pi\varepsilon_0\varepsilon k_B T$ is the Bjerrum length. Since the charge density is high, $\tau > 1$, the corresponding logarithmic electrostatic potential is strong enough to bind a certain portion of counterions to the aggregate surface, thus partially neutralizing the negative "bare" charge and replacing $\tau$ with a smaller $\tau_{eff}$ (the so-called Manning condensation[39]). The remaining charge is screened by a diffuse cloud of ions at Debye screening length $\lambda_D = e^{-1}\sqrt{\varepsilon\varepsilon_0 k_B T/N_A \sum_i c_{si} q_i^2}$; here $\varepsilon_0$ is the electric constant, $\varepsilon$ is the relative dielectric constant of water, $q$ is the ion's valency, "i" is the type of ion, $e$ is the elementary charge, $N_A$ is the Avogadro number. In the additive-free DSCG solution, $\lambda_D$ is determined by the "proper" counterions $Na^+$. For $c = 0.34$ mol kg$^{-1}$, $\lambda_D = 0.53$ nm, which leads to $\tau_{eff} = 2.7$.[40] The balance of the repulsive electrostatic forces and the osmotic pressure $\Pi$ imposed by the solution bath can be written, following ref. 38 and 41 as

$$\Pi = \sqrt{6\pi}\tau_{eff}^2 \frac{k_B T}{a^2 l_B K_1^2(a/\lambda)} \left(\frac{\lambda}{D}\right)^{3/2} \exp(-D/\lambda), \qquad (1)$$

where $K_1(x)$ is the first order modified Bessel function of the second type, $\lambda$ is the decay length, equal to $\lambda_D$ in the case of rigid rods. For flexible polyelectrolytes, fluctuative undulations leave the leading exponential dependence in eqn (1) intact, but the decay length is doubled, $\lambda = 2\lambda_D$, or quadrupled.[38,42] Eqn (1) predicts that to condense the DSCG solution with $c = 0.34$ mol kg$^{-1}$ and $\lambda = \lambda_D$ into a C phase with the hexagonal lattice period $D = 4$ nm, the osmotic pressure needs to be $\Pi \approx 10^5$ N m$^{-2}$; for a shorter $D = 3.5$ nm, the estimate is $\Pi \approx 4 \times 10^5$ N m$^{-2}$.

In our system, $\Pi$ is not known, but it can be associated with the additives accumulated in the I phase and estimated in an "ideal gas" model as $\Pi = [c_{Add}]N_A k_B T$. For Spm, assuming that Spm uses all the water in the solution, one finds $\Pi_{Spm} \approx (5 - 8) \times 10^5$ N m$^{-2}$. For PEG ($M_w$ 3350), using the tabulated data,[43] one finds $\Pi_{PEG} \approx (1.5 - 7) \times 10^5$ N m$^{-2}$. By the order of magnitude, these values match eqn (1).

(5) The condensed domains adopt non-spherical shapes, such as tactoids and toroids, Fig. 4. Tactoids are observed in variety of systems undergoing the I–N phase transition, see, *e.g.* ref. 24 and 25, while toroids are reported as a result of condensation of DNA with the hexagonal C order[12] and other stiff polyelectrolytes.[44]

The typical radius of DNA toroids is 50 nm, much smaller than the size of LCLC toroids.

Since $\hat{\boldsymbol{n}}(\boldsymbol{r})$ is tangential to the LC–I interface, the non-spherical shapes can be attributed to the balance of bulk LC elasticity and the surface tension $\sigma_{\|}$. For a constant volume $V \propto Rr^2 = \text{const}$ and a large aspect ratio $R/r$, the surface energy of both shapes scales as $F_S \propto \sigma_{\|} Rr \propto \sigma_{\|}\sqrt{RV}$, while the elastic energy scales as $F_e \propto KV/R^2$. Minimizing the sum $F_S + F_e$ with respect to $R$, one finds that for both shapes:

$$\frac{R}{r} = \alpha\left(\frac{K}{\sigma_{\|}}\right)^{3/5}\frac{1}{V^{1/5}}, \qquad (2)$$

where $\alpha$ is a geometrical factor on the order of 1; for toroids, $\alpha = 2^{1/5}\pi^{2/5} \approx 1.8$. The expression (2) agrees with more elaborate models considering tactoids[45] and toroids[46] separately. The modulus $K$ represents the bend elastic constant $K_{33}$ in the case of C toroids and is close to the splay constant $K_{11}$ in the case of N tactoids. For tactoids and toroids of volume (1–100) μm$^3$ to display an appreciable aspect ratio, say, $R/r = 2$, the ratio of material parameters $K/\sigma_{\|}$ which is of a dimension of length, should be macroscopic, ~1 to 10 μm. This estimate is orders of magnitude larger than the nanometre size of individual chromonic molecules, underlying a crucial importance of cooperative effects in the observed morphologies.

Both the surface and elastic energies in the consideration above scale as $F_S, F_e \propto V^{3/5}$. On the other hand, the energy of condensation, $F_{cond} \propto -\varepsilon V$ scales linearly with $V$; here $\varepsilon$ is the energy density difference between the bulk of the I and LC phases. Once large enough to overcome the barrier of nucleation, both toroids and tactoids should grow in size indefinitely. In our system, the condensed regions appear to stop their growth. One obvious reason is the depletion of the chromonic material in the surrounding I phase. The growth might be limited not only kinetically, but also thermodynamically, as reviewed for DNA toroids.[12] The issue is difficult to explore in the DNA because of the submicron scale of toroids. The chromonic toroids and tactoids, being on the scale of 10 μm, are readily accessible for studies by optical instruments and thus offer a unique opportunity to address the fascinating problem of nontrivial shape morphologies of self-assembled orientationally ordered systems. Note that the toroids are stable against unfolding into open bundles as long as the surface energy $2\pi r^2\sigma_{\perp}$ of the open ends exposed to water is larger than the bend energy $F_e$, i.e., for $\sigma_{\perp} \geq K / R \sim 10^{-6}$ J/m$^2$, a condition that is realistic, see Ref. 47.

## Conclusions

To conclude, we show experimentally the phenomenon of additives-induced condensation with ensuing orientational and positional ordering in lyotropic chromonic system in which small molecules are assembled by weak non-covalent forces in rich variety of morphologies, such as tactoids, bundles and giant toroids. The chromonic molecules are accumulated in the birefringent ordered domains while the non-aggregating additives are expelled into the isotropic disordered regions. The degree of this separation varies, depending on the nature of the additives. It is important to stress that the mesomorphic units in LCLCs are not rigid rods of fixed length. The crowding effect of additives is thus evident at two different levels. First, they assist in creating longer aggregates of DSCG that at some point became capable of forming a liquid crystalline state (even if the DSCG solution in the absence of the additives is isotropic). Second, the additives bring the aggregates closer together, inducing the higher packing density and forming a more densely packed nematic phase or a columnar phase within the condensed regions.

The aromatic planes of DSCG molecules in the condensed regions are on average perpendicular to the interface with the I phase. This feature, combined with the negative birefringence of the material and with the fact that the condensed C phase often shows toroids with $\hat{\boldsymbol{n}}$ that is parallel to the C–I interface (to allow bend but not splay nor twist deformations) points to the columnar type of aggregation, with the DSCG molecules being on average perpendicular to the director $\hat{\boldsymbol{n}}$.

Some of the features of chromonic condensation and segregation of components can be qualitatively explained by the Madden–Herzfeld[15,16] model of entropy-driven crowding. However, the model deals with the neutral species of spherical shape and is strictly speaking applicable only to the case of PEG. For Spm and TBABr, one needs to consider specific molecular interactions, such as the electrostatic attraction between the negatively charged DSCG and positively charged ions of these two additives that can penetrate the condensed regions. Furthermore, at present there is no theory capable to describe the tactoidal, toroidal and other morphologies of the condensed chromonic regions; these deserve further studies as they resemble closely the remarkable morphologies of biopolymer condensates such as DNA, but at the scales that allow one to perform optical microscopy studies.

## Acknowledgements

We thank A. Golovin, V. Nazarenko and O. Pishnyak for fruitful discussions. We acknowledge the role of Chithra Karunakaran and Martin Obst (CLS) for their excellence in maintaining the STXM instrument. The work was supported by NSF grants DMR 0906751, 086991, 0710544, 0706290 and 0606160, Ohio Board of Regents CMPND and ORS grants, W. M. Keck Foundation grant, MURI AFOSR FA9550-06-1-0337. Use of the Advanced Photon Source (APS) was supported by the US Department of Energy (DOE), Basic Energy Sciences (BES), Office of Science, under Contract No. W-31-109-Eng-38. The Midwestern Universities Collaborative Access Team's (MUCAT) sector at the APS is supported by the US DOE, BES, Office of Science, through the Ames Laboratory under Contract No. W-7405-Eng-82. The beam line X6B at NSLS is supported by the DOE under contract DE-AC02-98CHI0886. The Canadian Light Source (CLS) is supported by NSERC, CIHR, NRC and the University of Saskatchewan. Any opinions, findings, and conclusions or recommendations expressed in this publication are those of the author(s) and do not necessarily reflect the views of the National Science Foundation.

## References

1 J. E. Lydon, *Curr. Opin. Colloid Interface Sci.*, 2004, **8**, 480.
2 S.-W. Tam-Chang and L. Huang, *Chem. Commun.*, 2008, 1957.
3 A. J. Dickinson, N. D. LaRacuente, C. B. McKitterick and P. J. Collings, *Mol. Cryst. Liq. Cryst.*, 2009, **509**, 9.

 

4 D. J. Edwards, J. W. Jones, O. Lozman, A. P. Ormerod, M. Sintyureva and G. J. T. Tiddy, *J. Phys. Chem. B*, 2008, **112**, 14628.
5 M. Nakata, G. Zanchetta, B. D. Chapman, C. D. Jones, J. O. Cross, R. Pindak, T. Bellini and N. A. Clark, *Science*, 2007, **318**, 1276.
6 P. Mariani and L. Saturni, *Biophys. J.*, 1996, **70**, 2867.
7 L. J. Yu and A. Saupe, *Mol. Cryst. Liq. Cryst.*, 1982, **80**, 129.
8 A. F. Kostko, B. H. Cipriano, O. A. Pinchuk, L. Ziserman, M. A. Anisimov, D. Danino and S. R. Raghavan, *J. Phys. Chem. B*, 2005, **109**, 19126.
9 H. S. Park, S.-W. Kang, L. Tortora, Y. Nastishin, D. Finotello, S. Kumar and O. D. Lavrentovich, *J. Phys. Chem. B*, 2008, **112**, 16307.
10 L. Spindler, I. Drevenšek Olenik, M. Copic, J. Cerar, J. Škerjanc, R. Romih and P. Mariani, *Eur. Phys. J. E: Soft Matter Biol. Phys.*, 2004, **13**, 27.
11 E. Raspaud, M. Olvera de la Cruz, J.-L. Sikorav and F. Livolant, *Biophys. J.*, 1998, **74**, 381.
12 N. V. Hud and I. D. Vilfan, *Annu. Rev. Biophys. Biomol. Struct.*, 2005, **34**, 295.
13 H.-X. Zhou, G. Rivas and A. P. Minton, *Annu. Rev. Biophys.*, 2008, **37**, 375.
14 G. Zanchetta, M. Nakata, M. Buscaglia, T. Bellini and N. A. Clark, *Proc. Natl. Acad. Sci. U. S. A.*, 2008, **105**, 1111.
15 T. L. Madden and J. Herzfeld, *Mater. Res. Soc. Symp. Proc.*, 1992, **248**, 95.
16 T. L. Madden and J. Herzfeld, *Philos. Trans. R. Soc., A*, 1993, **344**, 357.
17 K. A. Simon, P. Sejwal, R. B. Gerecht and Y.-Y. Luk, *Langmuir*, 2007, **23**, 1453.
18 T. K. Attwood, J. E. Lydon, C. Hall and G. J. T. Tiddy, *Liq. Cryst.*, 1990, **7**, 657.
19 J. W. McBain, *Colloid Science*, D.C. Heath and Co., Boston, 1950, 450p.
20 I. S. Blagbrough and A. J. Geall, *Tetrahedron Lett.*, 1998, **39**, 439.
21 M. Shribak and R. Oldenbourg, *Appl. Opt.*, 2003, **42**, 3009.
22 K. V. Kaznatcheev, P. Dudin, O. D. Lavrentovich and A. P. Hitchcock, *Phys. Rev. E: Stat., Nonlinear, Soft Matter Phys.*, 2007, **76**, 061703.
23 N. H. Hartshorne and G. D. Woodard, *Mol. Cryst. Liq. Cryst.*, 1973, **23**, 343.
24 Yu. A. Nastishin, H. Liu, T. Schneider, T. V. Nazarenko, R. Vasyuta, S. V. Shiyanovskii and O. D. Lavrentovich, *Phys. Rev. E: Stat., Nonlinear, Soft Matter Phys.*, 2005, **72**, 041711.
25 P. W. Oakes, J. Viamontes and J. X. Tang, *Phys. Rev. E: Stat., Nonlinear, Soft Matter Phys.*, 2007, **75**, 061902.
26 E. I. Starostin, *J. Phys.: Condens. Matter*, 2006, **18**, S187.
27 A. S. Vasilevskaya, E. V. Generalova and A. S. Sonin, *Russ. Chem. Rev.*, 1989, **58**, 904; *Uspekhi Khimii*, 1989, **57**, 1575.
28 J. V. Champion and G. H. Meeten, *J. Pharm. Sci.*, 1973, **62**, 1589.
29 D. Goldfarb, Z. Luz, N. Spielberg and H. Zimmermann, *Mol. Cryst. Liq. Cryst.*, 1985, **126**, 225.
30 L. Wu, J. Lal, K. A. Simon, E. A. Burton and Y. Y. Luk, *J. Am. Chem. Soc.*, 2009, **131**, 7430.
31 W. L. Bragg and A. B. Pippard, *Acta Crystallogr.*, 1953, **6**, 865.
32 G. A. Stephenson and B. A. Diseroad, *Int. J. Pharmacol.*, 2000, **198**, 167.
33 A. Dembo, A. Ionov, P. Lazarev, A. Manko and V. Nazarov, *Mol. Mater.*, 2001, **14**, 275.
34 J. S. G. Cox, G. D. Woodard and W. C. McCrone, *J. Pharm. Sci.*, 1971, **60**, 1458.
35 M. P. Taylor and J. Herzfeld, *Phys. Rev. A: At., Mol., Opt. Phys.*, 1991, **43**, 1892.
36 A. J. Geall, R. J. Taylor, M. E. Earll, M. A. W. Eaton and I. S. Blagbrough, *Chem. Commun.*, 1998, 1403.
37 Y. Trukhina, S. Jungblut, P. Van der Schoot and T. Schilling, *J. Chem. Phys.*, 2009, **130**, 164513.
38 H. H. Strey, V. A. Parsegian and R. Podgornik, *Phys. Rev. E: Stat. Phys., Plasmas, Fluids, Relat. Interdiscip. Top.*, 1999, **59**, 999.
39 A. Naji, S. Jungblut, A. G. Moreira and R. R. Netz, *Physica A (Amsterdam)*, 2005, **352**, 131.
40 M. Aubouy, E. Trizac and L. Bocquet, *J. Phys. A: Math. Gen.*, 2003, **36**, 5835.
41 D. C. Rau, B. Lee and V. A. Parsegian, *Proc. Natl. Acad. Sci. U. S. A.*, 1984, **81**, 2621.
42 J. V. Selinger and R. F. Bruinsma, *Phys. Rev. A: At., Mol., Opt. Phys.*, 1991, **43**, 2922.
43 J. A. Cohen and S. Highsmith, *Biophys. J.*, 1997, **73**, 1689.
44 M. Gjertrud and B. T. Stokke, *Curr. Opin. Colloid Interface Sci.*, 2005, **10**, 16.
45 P. Prinsen and P. Van Der Schoot, *Eur. Phys. J. E: Soft Matter Biol. Phys.*, 2004, **13**, 35.
46 M. R. Stukan, V. A. Ivanov, A. Yu. Grosberg, W. Paul and K. Binder, *J. Chem. Phys.*, 2003, **118**, 3392.
47 V. G. Nazarenko, O. P. Boiko, H.-S. Park, O. M. Brodyn, M. M. Omelchenko, L. Tortora, Yu. A. Nastishin and O. D. Lavrentovich, *Phys. Rev. Lett.*, 2010, **105**, 017801.